

Oscillations of the black hole photon ring as a probe of ultralight dilaton fields

Chunlong Li,^a Chao Chen,^b Xiao Yan Chew^b

^aSchool of Physics, Hefei University of Technology, Hefei, Anhui 230009, China

^bSchool of Science, Jiangsu University of Science and Technology, Zhenjiang, 212100, China

E-mail: cchao012@just.edu.cn, xiao.yan.chew@just.edu.cn

Abstract. Recent advancements of very long baseline interferometry (VLBI) have facilitated unprecedented probing of superradiant phenomena in the vicinities of supermassive black holes (SMBHs), establishing an ideal laboratory to detect ultralight bosons beyond the Standard Model. In this study, we delve into how ultralight dilaton clouds, formed via SMBH superradiance, impact the black hole photon rings. Our focus is on the dilaton-electromagnetic coupling term of the form $f(\phi)F_{\mu\nu}F^{\mu\nu}$. By integrating geometric optics with plasma refractive effects in accretion environments, we demonstrate that the dilaton cloud dynamically alters the plasma frequency. Through systematic ray-tracing simulations covering a range of plasma densities and dilaton coupling strengths, we reveal a periodic distortion in the photon ring morphology, with the periodicity aligning with that of the dilaton-driven plasma frequency oscillations. We then assess the magnitude of this effect under the current angular resolution constraints of VLBI observations. Our analysis indicates that a comprehensive search for superradiant dilaton clouds based on the dilaton-electromagnetic coupling would necessitate radio interferometric baselines significantly exceeding the Earth's diameter to resolve the corresponding signatures.

Keywords: Ultralight bosons, Dilaton, Supermassive black holes, Superradiance

Contents

| | | |
|----------|--|-----------|
| 1 | Introduction | 1 |
| 2 | Superradiant dilaton cloud surrounding black holes | 2 |
| 3 | Photon propagation in the dilaton cloud and plasma | 3 |
| 4 | Simulation of the black hole photon ring | 6 |
| 4.1 | Ray-tracing algorithm | 6 |
| 4.2 | Results | 7 |
| 5 | Detectability of the dilaton-electromagnetic coupling | 9 |
| 6 | Conclusion | 11 |

1 Introduction

Taking advantage of the Very Long Baseline Interferometer (VLBI) technology, the Event Horizon Telescope (EHT) opens a new era of probing physics under extreme conditions near the horizon of a supermassive black hole (SMBH) [1–4]. The capture of black hole images offers us the potential to explore new physics within a strong gravitational field. In the center of the galaxy M87, the compact radio source is resolved as an asymmetric bright emission disk, which encompasses a central dark region. In the current literature, although the details remain to be examined, it is pointed out that there could exist a strong lensing structure which is called “photon ring” behind the dominated direct emission profile from the accretion disk [5, 6]. With the help of sufficient high-resolution imaging, complexities from astrophysical effects can be mitigated, as the size and shape of the photon ring are totally determined by the instabilities of photon orbits predicted by geodesic equations, which makes the black hole photon ring potential probe to test the effect of strong gravity and related new physics [7–11].

Besides the applications to test gravity, such horizon-scale measurements also provide us opportunities to test particle physics, especially ultralight bosons. This kind of particles generically appear in theories with extra dimensions [12], and they can be good cold dark matter candidates [13–15]. With a proper mass, ultralight bosonic particles can be spontaneously accumulated around a supermassive Kerr black hole through the superradiance mechanism [16–24]. During this process, the growth and temporal oscillations of the superradiant boson cloud perturb the surrounding spacetime, thereby imprinting observable signatures on the black hole shadow or photon ring [25–28]. Beyond gravitational effects, superradiant bosons may also generate detectable signals through non-gravitational couplings to Standard Model particles. In [29], the EHT polarimetric measurement on M87* is proposed to search for the existence of the superradiance axion particles through the birefringence effects induced by their coupling with photons [30, 31]. The coherently oscillating axion field will lead to a periodic variation to the electric vector position angles of linearly polarized radiations from the accretion flow, making the extraction of this phenomenon from the polarimetric measurement on supermassive black holes a potential tool to tightly constrain the axion parameter space [32, 33].

The dilaton, as another hypothetical ultralight bosonic field, plays a significant role in theoretical cosmology. In string theory-inspired models, the dilaton arises naturally as a scalar partner to the graviton, governing the strength of gravitational interactions through its coupling to spacetime geometry [34, 35]. It has been proposed as a candidate for driving dynamical dark energy, offering a mechanism for the late-time accelerated expansion of the universe [36, 37]. The time-dependent vacuum expectation value of the dilaton field could also imprint observable signatures on the cosmic microwave background (CMB) anisotropies or large-scale structure formation [38, 39]. Additionally, the dilaton may also mediate variations of fundamental constants (e.g., the fine-structure constant) over cosmic time, which could be tested via astrophysical observations [40–42]. Given its rich theoretical and phenomenological properties, it is imperative to expand the range of search strategies for the dilaton.

In this work, we focus on the dilaton cloud formed via the superradiant mechanism around supermassive black holes. Our starting point is the coupling term $f(\phi)F_{\mu\nu}F^{\mu\nu}$ between dilaton and the electromagnetic field. Using the geometric optics approximation, we derive the dispersion relation governing photon propagation under the influence of the superradiant dilaton field, demonstrating that the presence of the dilaton modifies the effective mass term of photons contributed by the plasma frequency. Through ray-tracing numerical simulations, we model the impact of this effect on the morphology of the black hole photon ring, revealing periodic oscillations in its shape and size with a period matching the oscillation cycle of the superradiant dilaton field. Furthermore, under a pressureless perfect fluid spherically symmetric accretion model, we estimate the magnitude of this effect, indicating that significantly longer radio interferometric array baselines would be required to observe such signatures.

The structure of this paper is as follows. In Section 2, we briefly review the superradiance mechanism of black holes. In Section 3, we derive the modified dispersion relation and equations of motion for photons under the influence of the dilaton field. In Section 4, we employ a ray-tracing computational code to simulate the resulting modifications in the photon ring morphology. In Section 5, we assess the observability of the superradiant dilaton field under current instrumental sensitivity thresholds. Section 6 concludes with a summary and discussion of implications. Throughout this study, we work in units where $G = \hbar = c = 1$, and adopt the metric convention $(-, +, +, +)$.

2 Superradiant dilaton cloud surrounding black holes

The superradiance mechanism involves a comparison between two physical scales. One is the boson’s reduced Compton wavelength λ_c , which is related to the boson mass μ through $\lambda_c \equiv 1/\mu$, the other is the gravitational radius $r_g \equiv M$ with M be the mass of the Kerr black hole. When λ_c is comparable to r_g , the superradiance mechanism takes effect, generating an exponentially growing boson cloud [16–24]. For supermassive black holes with masses ranging from $10^6 M_\odot$ to $10^{10} M_\odot$, the boson mass μ falls within the range of 10^{-20}eV to 10^{-16}eV , which is well within the ultralight regime. By ignoring the dilaton self-interaction, the Klein–Gordon equation of dilaton field in a curved spacetime takes the form

$$(\nabla^\mu \nabla_\mu - \mu^2)\phi = 0 . \quad (2.1)$$

Here, ∇_μ is taken as the covariant derivative in terms of the Kerr metric of rotating black holes, with the mass M and the angular momentum J in Boyer-Lindquist (BL) coordinates

$x^\mu = [t, r, \theta, \varphi]$. Under this condition, the solution to Eq. (2.1) exhibits separability of variables and can be expressed in the following form [43, 44],

$$\phi(t, \mathbf{r}) = e^{-i\omega t + im\varphi} R_{nlm}(r) S_{lm}(\theta) , \quad (2.2)$$

where $R_{nlm}(r)$ is the radial function, $S_{lm}(\theta)$ is the spheroidal harmonics which simplifies to the spherical harmonics Y_{lm} in the non-rotating limit of the black hole. The eigenstates ω_{nlm} of the system are labeled by quantum numbers (n, l, m) satisfying $n \geq l + 1, l \geq 0$ and $l \geq |m|$. The boundary condition of the wavefunction is the ingoing at the Kerr black hole's outer horizon and going to zero at infinity, which makes the eigen-frequencies ω generally take a complex form $\omega_{nlm} = \omega_{nlm}^r + i\omega_{nlm}^i$. The onset of superradiance can be clearly demonstrated by considering the regime where the dimensionless coupling parameter $\alpha \equiv r_g/\lambda_c$ satisfies $\alpha \ll 0.1$. In this limit, the real part ω_{nlm}^r and the imaginary part ω_{nlm}^i can be written as [21, 45]

$$\omega_{nlm}^r = \mu \left(1 - \frac{\alpha^2}{2n^2} + \mathcal{O}(\alpha^4) \right) , \quad (2.3)$$

$$\omega_{nlm}^i \propto \alpha^{4l+5} (m\Omega_H - \omega_{nlm}^r) (1 + \mathcal{O}(\alpha)) , \quad (2.4)$$

where $\Omega_H \equiv a/(2r_+)$ with the radius of the outer horizon as $r_+ \equiv r_g + r_g\sqrt{1-a^2}$ and the dimensionless spin as $a \equiv J/M^2$. The higher order terms of α can be found in [46], which contains the dependence on the quantum number l and m . According to Eq. (2.4), when the black hole spin, the boson mass μ and the gravitational radius r_g satisfy

$$\Omega_H > \frac{\omega_{nlm}^r}{m} , \quad (2.5)$$

ω_{nlm}^i can be positive for a particular set of quantum numbers n, l and m . This leads to an exponential growth with the timescale as $\tau_{SR} = 1/\omega_{nlm}^i$, i.e., the superradiance process.

We then discuss the radial component $R(r)$ of the wavefunction. For generic values of α , $R(r)$ generally requires numerical calculations to obtain its profile. According to the numerical study in [23], the state with the lowest energy state among the ones satisfying the superradiance condition has the highest superradiant rate, which corresponds to $n = 2, l = 1, m = 1$ and $S_{11}(\theta) = \sin\theta$, peaking at the equatorial plane ($\theta = 90^\circ$) of the black hole. In this work, we adopt this state as our benchmark, whose explicit form is given by:

$$\phi(t, \mathbf{r}) = \phi_{\max} e^{-i\omega t + im\varphi} \mathcal{R}_{211}(r) \sin(\theta) , \quad (2.6)$$

where \mathcal{R}_{211} is defined as $\mathcal{R}_{211}(r) \equiv R_{211}(r)/R_{211}(r_{\max})$ with r_{\max} denoting the radius at which the radial profile $R(r)$ reaches its maximum, and ϕ_{\max} is the corresponding maximum field value. In the limit of $\alpha \ll 0.1$, $r_{\max} \approx n^2/(2\alpha^2)r_g$. In Fig. 2, the radial profile $\mathcal{R}_{211}(r)$ for certain values of α and $a = 0.99$ is displayed. The derivative $\mathcal{R}'_{211}(r)$ is also displayed since it is related to the dilaton-induced plasma effect discussed subsequently.

3 Photon propagation in the dilaton cloud and plasma

The dilaton field ϕ couples non-minimally to the electromagnetic field tensor $F_{\mu\nu} = \partial_\mu A_\nu - \partial_\nu A_\mu$ via a Lagrangian interaction term of the form

$$\mathcal{L} = -\frac{1}{4}f(\phi)F_{\mu\nu}F^{\mu\nu} - eA_\mu J^\mu , \quad (3.1)$$

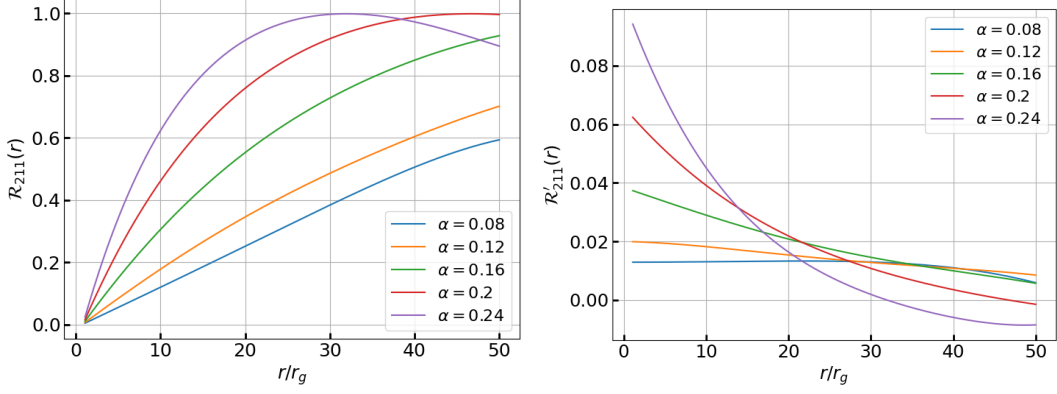


Figure 1. Left: The figure shows the radial profile $\mathcal{R}_{211}(r)$ of the wavefunction for $a = 0.99$ obtained from the numerical result. **Right:** The derivative of $\mathcal{R}_{211}(r)$ with respect to the radial coordinate r .

as derived from the low-energy effective action of string theory with $f(\phi) = e^{-2\phi}$ [35]. We incorporate the electromagnetic four-current $J^\mu = (\rho, \vec{J})$, generated by the collective motion of electrons (with e denoting the elementary charge), to self-consistently account for plasma effects within the accretion environment. For protons, their mass is approximately three orders of magnitude larger than that of electrons, rendering their collective motion dynamically negligible in most astrophysical plasma scenarios [47]. Assuming $F_{\mu\nu}$ describes the photon electromagnetic field, the interaction Lagrangian implies that a slowly varying dilaton background modifies photon propagation via its coupling to $F_{\mu\nu}F^{\mu\nu}$. To systematically capture these corrections, our method is based on the geometric optics approximation [48]. By choosing $f(\phi) = 1 - \epsilon\phi$ as a benchmark model, where ϵ is the coupling constant between ϕ and $F_{\mu\nu}$, we start from the Maxwell equations in flat spacetime derived by varying the Lagrangian (3.1),

$$\nabla \cdot \vec{E} = \epsilon(1 - \epsilon\phi)^{-1} \nabla\phi \cdot \vec{E} + \rho(1 - \epsilon\phi)^{-1}, \quad (3.2)$$

$$\nabla \times \vec{B} - \frac{\partial \vec{E}}{\partial t} = \epsilon(1 - \epsilon\phi)^{-1} \left(\nabla\phi \times \vec{B} - \frac{\partial \phi}{\partial t} \vec{E} \right) + \vec{J}(1 - \epsilon\phi)^{-1}, \quad (3.3)$$

$$\nabla \times \vec{E} + \frac{\partial \vec{B}}{\partial t} = 0, \quad (3.4)$$

$$\nabla \cdot \vec{B} = 0, \quad (3.5)$$

which leads to the modified Helmholtz equation:

$$\begin{aligned} \nabla^2 \vec{E} - \frac{\partial^2 \vec{E}}{\partial t^2} &= \epsilon^2 (1 - \epsilon\phi)^{-2} \left(\frac{\partial \phi}{\partial t} \nabla\phi \times \vec{B} - \left(\frac{\partial \phi}{\partial t} \right)^2 \vec{E} + \nabla\phi \cdot (\nabla\phi \cdot \vec{E}) \right) \\ &+ \epsilon (1 - \epsilon\phi)^{-1} \left(\nabla \frac{\partial \phi}{\partial t} \times \vec{B} - \frac{\partial^2 \phi}{\partial t^2} \vec{E} + \vec{E} \times (\nabla \times \nabla\phi) + (\vec{E} \cdot \nabla) \nabla\phi \right) \\ &+ (1 - \epsilon\phi)^{-1} \left(\frac{\partial \vec{J}}{\partial t} + \nabla\rho \right) + \epsilon (1 - \epsilon\phi)^{-2} \left(\frac{\partial \phi}{\partial t} \vec{J} + \rho \nabla\phi \right) \\ &+ \epsilon (1 - \epsilon\phi)^{-1} \left((\nabla\phi \cdot \nabla) \vec{E} - \frac{\partial \phi}{\partial t} \frac{\partial \vec{E}}{\partial t} \right). \end{aligned} \quad (3.6)$$

Although the equation's mathematical complexity resists analytical approaches, the geometric optics limit can dramatically simplify the system. This approximation is formally implemented by positing a solution of the form

$$\vec{E} = \vec{E}_0 e^{iS}, \quad \vec{B} = \vec{B}_0 e^{iS}, \quad (3.7)$$

and defined by the requirement that the variation scale of phase S is much smaller than the variation scale of amplitude $\vec{E}_0(\vec{B}_0)$ over the spacetime. This requirement implies that the photon wavelength λ must be much smaller than the characteristic length scale L of other background fields in the system ($\lambda \ll L$). For the non-relativistic dilaton field formed by the superradiance process, the radio band photons generally satisfy $1/\lambda \gg \mu \gg k_\phi \sim 1/r_g$, where k_ϕ is characterized by $k_\phi \sim |\nabla\phi|/\phi$. Then we consider the variation scale of the current (ρ, \vec{J}) . The charge density and current density are related through the plasma continuity equation:

$$\frac{\partial \rho}{\partial t} + \nabla \cdot \vec{J} = 0, \quad (3.8)$$

where the current density \vec{J} is driven by the electric field \vec{E} , which is expressed as $\vec{J} = i\omega_p^2/\omega \vec{E}$ for photons with a specific frequency ω [49]. ω_p is the plasma frequency, which is determined by the number density of electrons n_e through the relation $\omega_p^2 = n_e e^2/m_e$ with m_e be the electron's mass. Given that the collective motion of plasma near the black hole is predominantly governed by gravitational forces, the characteristic scale $k_e \sim |\nabla n_e|/n_e$ of plasma density variations should align with the gravitational radius r_g , i.e., $k_e \sim 1/r_g$. For instance, in various accretion disk models, the electron number density n_e is commonly assumed to follow a power-law dependence on radius r , i.e., $n_e(r) \propto (r/r_g)^h$, where h is a model-dependent index [50]. By substituting the solution form (3.7) into Eq.(3.6), the condition $1/\lambda \gg k_\phi, k_e$ means all the derivatives of ϕ , ω_p and the amplitude \vec{E}_0, \vec{B}_0 can be neglected under the lowest order geometric optics approximation, which makes Eq.(3.6) reduce into

$$-E_j k_\mu k^\mu = \omega_p^2 E_j (1 - \epsilon\phi)^{-1}, \quad (3.9)$$

where $k^\mu = (\omega, \vec{k})$ is defined as $\omega \equiv -\dot{S}$, $\vec{k} \equiv \nabla S$. The existence of solutions to Eq.(3.9) requires the operator acting on \vec{E} to vanish, i.e., the following quantity must satisfy:

$$\mathcal{H} = \vec{k}^2 - \omega^2 + \omega_p^2 (1 - \epsilon\phi)^{-1}. \quad (3.10)$$

In the Hamiltonian formalism of geometric optics [48, 51], the constraint $\mathcal{H} = 0$ must hold along photon worldlines, governing their trajectories, and also can be regarded as the dispersion relation followed by photons. This modified dispersion relation dynamically couples the photon's effective mass — originating from plasma interactions — to the ambient dilaton field. One could expect the temporal oscillations in the dilaton background induce periodic modulations of this effective mass, thereby perturbing photon trajectory evolution and imprinting detectable signatures in observable quantities such as black hole photon ring morphology.

Finally, we consider the effect of the gravitational field. The minimal coupling between gravity and the photon field can be conveniently incorporated into the Lagrangian (3.1). Based on the condition $\lambda \ll r_g$ and the same geometric optics approximation strategy as in the previous discussion, all derivative terms of the metric can be neglected in the process of

simplifying the equations of motion. This implies that the effect of gravity can be included by replacing $\eta_{\mu\nu}$ with $g_{\mu\nu}$, i.e.,

$$\mathcal{H} = \frac{1}{2} (g^{\mu\nu} k_\mu k_\nu + \omega_p^2 (1 - \epsilon\phi)^{-1}) . \quad (3.11)$$

From this we can trace rays via a system of Hamiltonian optics equations

$$\frac{dx^\mu}{d\lambda} = \frac{\partial \mathcal{H}}{\partial k_\mu}, \quad \frac{dk_\mu}{d\lambda} = -\frac{\partial \mathcal{H}}{\partial x^\mu}, \quad (3.12)$$

where λ is an arbitrary world line parameter. Eqs. (3.12) gives the modified geodesic equation

$$\frac{d^2 x^\sigma}{d\lambda^2} + \Gamma_{\mu\nu}^\sigma \frac{dx^\mu}{d\lambda} \frac{dx^\nu}{d\lambda} + \frac{1}{2} g^{\rho\sigma} \frac{\partial}{\partial x^\rho} (\omega_p^2 (1 - \epsilon\phi)^{-1}) = 0 . \quad (3.13)$$

4 Simulation of the black hole photon ring

4.1 Ray-tracing algorithm

In order to extract observational signal of superradiance dilaton cloud from the supermassive black hole images, we employ the ray-tracing algorithm to compute the photon ring images of a Kerr black hole surrounded by the superradiance dilaton cloud and plasma. To this end, we assume that photons are emitted from the observer's image plane, following the trajectory described by Eq. (3.12), then scattered by the black hole. Finally, based on the reversibility of light paths, we obtain the propagation path of this light ray reaching the image plane.

The location of the observer is denoted as (r_o, θ_o, ϕ_o) in Boyer-Lindquist spherical coordinates of Kerr black holes. We consider the observer is far away from the black hole, where the spacetime is well described by Minkowski metric. In the observer's reference frame, the coordinates of a point in the image space are labeled as (X, Y, Z) , which is related to the Cartesian coordinate (x, y, z) of Boyer-Lindquist coordinates through the following relationship

$$\begin{aligned} x &= r_o \sin \theta_o + Z \sin \theta_o - Y \cos \theta_o , \\ y &= X , \\ z &= r_o \cos \theta_o + Z \cos \theta_o + Y \sin \theta_o , \end{aligned} \quad (4.1)$$

where we have set $\phi_o = 0$ for simplicity. The transformation between the Boyer-Lindquist Cartesian and spherical coordinates is given as

$$\begin{aligned} r &= \sqrt{x^2 + y^2 + z^2} , \\ \theta &= \arccos \frac{z}{r} , \\ \phi &= \arctan \frac{y}{x} . \end{aligned} \quad (4.2)$$

By combining Eq. (4.1) and Eq. (4.2), any point $(X, Y, 0)$ in the observer's image plane can be expressed in Boyer-Lindquist spherical coordinates (r, θ, ϕ) of black holes, which will serve as the initial coordinate condition for the ray-tracing algorithm. As for the initial momenta $(\dot{r}, \dot{\theta}, \dot{\phi})$, the derivative with respect to affine parameter λ of Eq. (4.2) gives rise to

$$\begin{aligned} \dot{r} &= \dot{Z} \cos \theta \cos \theta_o - p_0 \sin \theta \sin \theta_o \cos \phi , \\ \dot{\theta} &= \frac{\dot{Z}}{r} [\sin \theta_o \cos \theta \cos \phi - \sin \theta \cos \theta_o] , \\ \dot{\phi} &= -\frac{\dot{Z}}{r \sin \theta} \sin \theta_o \sin \phi . \end{aligned} \quad (4.3)$$

Here, we consider light rays emitted perpendicular to the image plane, i.e., $\dot{X} = \dot{Y} = 0$.

As for \dot{t} , the Hamiltonian condition $\mathcal{H} = 0$ gives

$$\dot{t} = \beta + \sqrt{\beta^2 + \gamma}, \quad (4.4)$$

$$\beta \equiv -\frac{g_{ti}\dot{x}^i}{g_{tt}}, \quad \gamma \equiv -\frac{g_{ij}\dot{x}^i\dot{x}^j + \omega_p^2(1 - \phi(\vec{x}, t))^{-1}}{g_{tt}}. \quad (4.5)$$

With the initial condition given above, we integrate the second-order differential equations (3.13) backwards using a second-order Runge-Kutta integrator. The integration goes on until photons fall into the black hole or escape to infinity. In order to maintain numerical precision near the event horizon and improve the efficiency, we adopt a variable step size strategy. At each integration step, we compute the rates of change in the (r, θ, ϕ) directions. The final adaptive step size is determined by taking the harmonic mean of these directional rates of change, constrained by prescribed upper and lower bounds to ensure numerical stability and precision.

4.2 Results

The black hole photon ring corresponds to the gravitationally lensed image of the photon capture region, where photons occupy unstable orbits with constant radii. In static spherically symmetric spacetimes (e.g., Schwarzschild geometry), this region collapses to a photon sphere, a critical spherical surface at $r = 3r_g$. Perturbations off these marginally stable orbits exhibit exponential divergence governed by the Lyapunov exponent, bifurcating trajectories into escaping to distant observers or plunging across the event horizon [5]. Photons completing multiple near-critical orbits prior to escape experience extreme gravitational lensing and Doppler boosting, producing the characteristic photon ring substructure as

$$I^{\text{obs}}(X, Y) = \sum_m g(r)^4 I(r) \Big|_{r=r_m(X, Y)}, \quad (4.6)$$

where $r_m(X, Y)$ denotes the radial coordinate of the m^{th} intersection with the disk plane outside the horizon, $I(r)$ is the emission profile of the disk, and $g(r)$ represents the redshift factor. For an extreme Kerr black hole with $a = 0.99$ and $\theta_o = \pi/2$, the orange region in the left panel of Fig. 2 numerically demonstrates $n \geq 2$ photon subrings without considering the effects of plasma and the dilaton coupling. The blue contour lines represent the polynomial fit to this region, while the red dashed lines denote the analytic solution for the photon ring in the $n \rightarrow \infty$ limit. As shown, the two results exhibit remarkable agreement for observers at $\theta_o = \pi/2$. In the following analysis, we fix the black hole spin to $a = 0.99$ and the inclination to $\theta_o = \pi/2$. Our focus lies on the photon subring morphology defined by orbits with $n \geq 2$, corresponding to the photon trajectories passing through the accretion disk twice.

As for the plasma frequency, we adopt a power-law profile

$$\omega_p^2 = \frac{k_0^2}{r^h}. \quad (4.7)$$

The power-law index h typically depends on fluid dynamics, accretion rate, black hole mass, and other parameters. For the radiatively inefficient accretion flow (RIAF) model, the typical value of h is 1.5 [52]. In the right panel of Fig. 2, the photon ring contours formed by different photon frequencies p_0/k_0 for $h = 1$ are plotted. It can be observed that the lower the photon

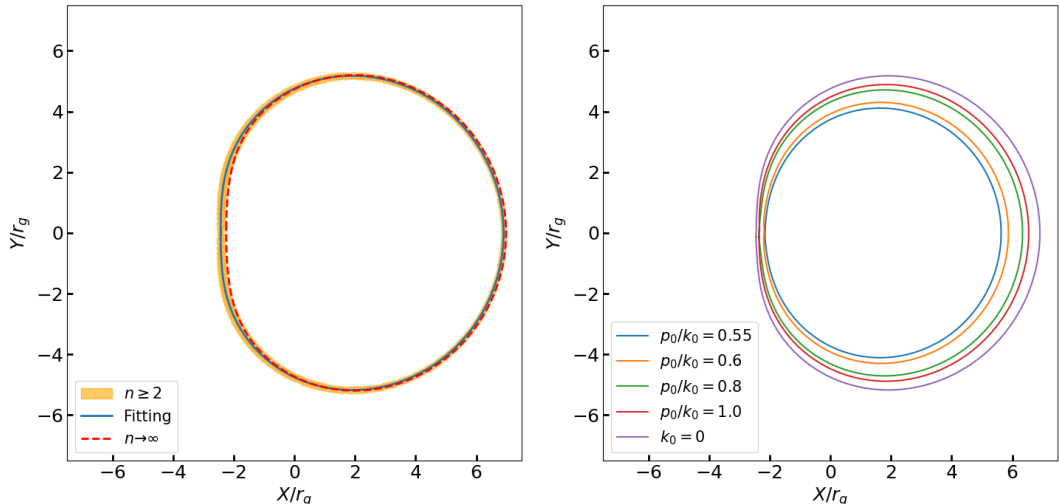


Figure 2. Left: The figure shows the photon ring obtained from the analytical result for $n \rightarrow \infty$ (red dashed line), as well as the region enclosed by the photon subrings with $n \geq 2$ in the case of $k_0 = 0$, $a = 0.99$ and $\theta_o = \pi/2$ (orange). A polynomial fitting method was used to fit this region with a smooth curve (blue), which closely approximates the contour of the $n \rightarrow \infty$ photon ring. **Right:** For $a = 0.99$ and $\theta_o = \pi/2$, the photon ring contours formed by different photon frequencies p_0 , which enters the numerical computation through the ratio p_0/k_0 .

frequency, the smaller the resulting ring size, which is consistent with the conclusions from previous studies [53].

Next, we take into account the dilaton field generated by superradiance. Unlike the usual ray-tracing results, the propagation path of photons depends on their departure time on the image plane, which is caused by the time-oscillating effect of the dilaton field. In Fig. 3, we illustrate the evolution of the photon ring over time for different values of p_0/k_0 and $A \equiv \epsilon\phi_{\max}$, with the temporal sequence indicated by rainbow colors. It can be observed that, under the influence of the dilaton field, the shape and size of the photon ring undergo periodic changes, with the period matching the oscillation period $T \equiv 2\pi/\alpha$ of the dilaton field. The extent of the photon ring's modification reaches its maximum at approximately $0.5T$. As p_0/k_0 decreases, indicating an enhancement of the plasma effect, the amplitude of the photon ring's variation increases. This aligns with the implication of Eq. (3.13): the dilaton manifests its effect by altering the plasma frequency, and thus the strength of its effect depends on the magnitude of the plasma frequency. Moreover, the degree of change in the photon ring's shape increases with A , which is consistent with the intuitive conclusion that a larger dilaton field leads to stronger effects.

Then we discuss the impact of the dilaton mass μ on the distortion effect of the photon ring. In Fig. 4, we illustrate the temporal oscillations of the photon ring for different values of $\alpha = \mu r_g$. We find that the oscillation amplitude of the photon ring does not exhibit a monotonic dependence on α , which results from the interplay of multiple factors. First, as α increases, the radial location r_{\max} of the maximum value of the dilaton wavefunction decreases. This leads to a larger dilaton wavefunction and its radial derivative in the photon capture region ($r_g \leq r \leq 4r_g$ for $a = 1$) according to Eq. (3.13), enhancing the effect of the dilaton field. Meanwhile, a larger α corresponds to a shorter oscillation period of the dilaton field. As a result, during numerical integration, the effects induced by the oscillating field

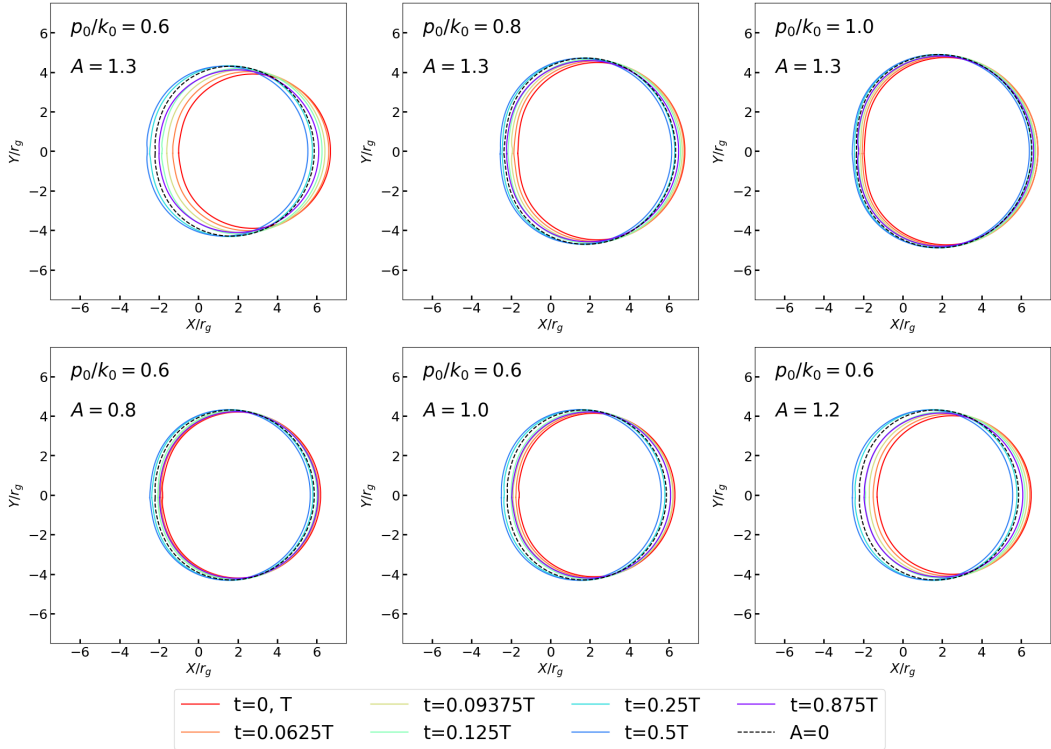


Figure 3. The figure shows the evolution of the photon ring over time for different values of p_0/k_0 and $A = \epsilon\phi_{\max}$, where $T \equiv 2\pi/\alpha$ represents the oscillation period of the superradiant dilaton field. Different rainbow colors represent the temporal sequence of evolution. The black dashed line represents the case without the dilaton field ($A = 0$). The black hole spin and inclination are fixed at $a = 0.99$, $\theta_0 = \pi/2$.

values tend to average out, weakening the overall impact, which is similar to that encountered in birefringence-based searches for superradiant axion clouds [32, 33]. Additionally, when the maximum value of the dilaton field, characterized by parameter A , is large, the nonlinear dependence of the dilaton coupling term in Eq. (3.13) becomes significant. This weakens the linear dependence of the effect on the parameters. These three factors collectively lead to the non-monotonic dependence of the photon ring oscillation amplitude on α . In the next manuscript, we will include corresponding schematic diagrams to illustrate these three points in detail.

5 Detectability of the dilaton-electromagnetic coupling

In this section, we provide an order-of-magnitude estimate of the distortion of the photon ring caused by the superradiance dilaton cloud, in order to assess the detectability of this phenomenon. For the motion of photons, we ignore the spin of the black hole for simplicity and assume the metric to be the Schwarzschild metric. We first start with the radius d of the photon ring of a Schwarzschild black hole as observed at infinity, incorporating plasma effects that follow Eq. (4.7), which is given by the expression [54]:

$$\frac{d}{r_g} = 3\sqrt{3}(1 - \delta_p), \quad \delta_p \equiv 3^{-h-1} \frac{k_0^2}{\omega_0^2}. \quad (5.1)$$

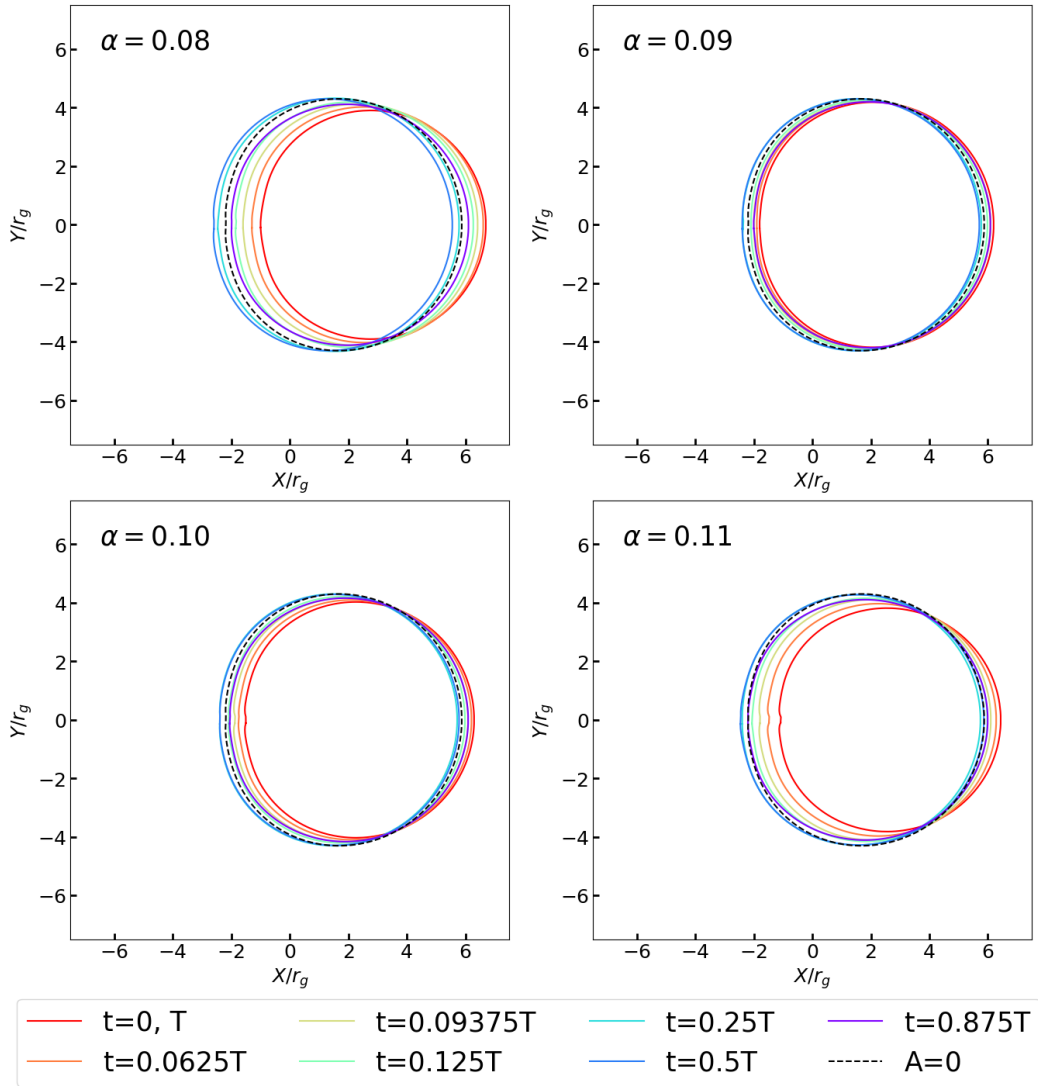


Figure 4. The figure shows the time evolution of the photon ring for different values of α , with A fixed at 1.3 and p_0/k_0 fixed at 0.6. The black hole spin and inclination are fixed at $a = 0.99$, $\theta_0 = \pi/2$.

According to Eq. (3), the effect of the dilaton field is equivalent to modifying the plasma frequency. This modification introduces additional dependencies on t, r, θ, ϕ , making the photon motion equations no longer separable and thus difficult to solve. However, when α is much smaller than 0.1, the oscillation period of the dilaton field, $T_\phi = 2\pi/\alpha$, is much longer than the orbital period of the photon, $T_s \approx 2\pi r_s$ with $r_s = 3r_g$ being the radius of the unstable circular photon orbit in Schwarzschild spacetime. Therefore, the influence of the dilaton field on the photon can be regarded as a quasi-static process. That is, for photons reaching the image plane at a specific moment, the dilaton field they experience during their motion near the black hole can be considered independent of the coordinate time t . Furthermore, considering that the photons forming the photon ring spend most of their trajectories near the unstable circular orbit at r_s , the correction to their trajectories is primarily determined by the field value at r_s , i.e., $R_{211}(r_s)$. Based on the above considerations, by neglecting

the dependence of ϕ on θ and φ , the dilaton field can be approximated as a constant $\epsilon\bar{\phi}$ as a leading-order estimate of its distortion effect on the photon ring, where $\bar{\phi}$ represents the typical field value near r_s , which leads to the modified photon ring radius

$$\frac{d}{r_g} = 3\sqrt{3}(1 - \delta_p - \delta_\phi), \quad \delta_\phi \equiv 3^{-h-1} \frac{k_0^2}{\omega_0^2} \epsilon\bar{\phi}. \quad (5.2)$$

As an example, we consider that the plasma electron density corresponds to the spherically symmetric accretion of a perfect fluid without pressure [55]. In this situation, $h = 1.5$ in Eq. (4.7), and k_0^2 is given by [56]

$$k_0^2 = \frac{e^2 L}{\sqrt{2}\eta m_e m_p r_g^2}, \quad (5.3)$$

where e is the electric charge, m_e and m_p are the mass of the electron and proton respectively, L is the observed luminosity of the galactic center, and η is the non-dimensional coefficient characterizing the accretion efficiency. Based on Eqs. (5.2), (5.3), the magnitude of $\epsilon\bar{\phi}$ can be estimated as

$$\epsilon\bar{\phi} = 10^{-4} \left(\frac{\delta_\phi}{0.01} \right) \left(\frac{\eta}{10^{-4}} \right) \left(\frac{\lambda_0}{100\text{cm}} \right)^{-2} \left(\frac{L}{10^6 L_\odot} \right)^{-1} \left(\frac{M}{4 \times 10^6 M_\odot} \right)^2. \quad (5.4)$$

Here, L and M are taken as the values of the Galactic central black hole Sgr A* [57–59]. For the central black hole of M87, these values are $L = 1.8 \times 10^7 L_\odot$ and $M = 6.5 \times 10^9 M_\odot$ [60–62]. η is taken as the value of the advection-dominated accretion flows model, with a range that can span from 10^{-4} to 0.1 [52, 63, 64]. Considering that in observational bands above the millimeter range, the photon ring of Sgr A* would be washed out by scattering [65], we choose $\lambda = 100\text{cm}$. According to Eq. (5.2), smaller observational wavelengths are also advantageous for detecting the dilaton field. The photon ring distortion $\delta\phi$ can be converted into the corresponding change $\delta\beta$ in angular size using $\beta = \delta_\phi/r_o$, where r_o is the distance to the black hole. For $\delta_\phi = 0.01$ and $r_o = 8.3\text{kpc}$ of the distance of Sgr A*, $\delta\beta = 2.4 \times 10^{-3} \mu\text{as}$. For comparison, at the $\lambda = 1.3\text{mm}$ wavelength, the Event Horizon Telescope (EHT), with Earth’s diameter $D \approx 1.3 \times 10^4\text{km}$ as its aperture, has an angular resolution of $\delta\beta = \lambda/D \approx 20\mu\text{as}$ [1]. Therefore, to test the effects induced by the dilaton field based on its electromagnetic coupling, a longer baseline length is required.

6 Conclusion

In this manuscript, we systematically investigated the imprints of superradiant dilaton clouds on black hole photon rings through dilaton-electromagnetic coupling. By combining geometric optics with plasma refractive effects, we demonstrated that the coherent oscillations of the dilaton cloud dynamically modulate the effective plasma frequency, imprinting periodic distortions on the photon ring morphology with a characteristic periodicity matching the dilaton field’s oscillation cycle. Ray-tracing simulations revealed that the distortion amplitude depends sensitively on plasma density, dilaton coupling strength, and the dimensionless mass parameter α , the latter exhibiting non-monotonic behavior due to competing effects between the dependence of the wavefunction on α and the averaging effect of integration over the dilaton oscillations. Our order-of-magnitude estimates indicate that resolving these signatures for SMBH like Sgr A* or M87* would require radio interferometric baselines exceeding

the Earth’s diameter, highlighting the necessity for next-generation space-based VLBI arrays to probe ultralight dilatons based on its electromagnetic coupling through photon ring oscillations. This work establishes photon ring dynamics as a novel observable for testing superradiance-induced new physics beyond gravitational interactions.

Acknowledgments

We are grateful for useful discussions with Changhong Li and Yue Zhao, which inspired the key ideas presented in this manuscript. CL is supported by National Natural Science Foundation of China (No. 12447128) and the China Postdoctoral Science Foundation (No. 2024M760720). CC is supported by National Natural Science Foundation of China (No. 12433002) and Start-up Funds for Doctoral Talents of Jiangsu University of Science and Technology. CC thanks the supports from The Asia Pacific Center for Theoretical Physics, The Center for Theoretical Physics of the Universe at IBS, The COSPA Group at the USTC during his visits. XYC is supported by the starting grant of Jiangsu University of Science and Technology (JUST). All numerics are operated on the computer clusters in the cosmology group at IAS, HKUST.

References

- [1] K. Akiyama *et al.* (Event Horizon Telescope), *Astrophys. J. Lett.* **875**, L1 (2019), [arXiv:1906.11238 \[astro-ph.GA\]](#) .
- [2] K. Akiyama *et al.* (Event Horizon Telescope), *Astrophys. J. Lett.* **875**, L4 (2019), [arXiv:1906.11241 \[astro-ph.GA\]](#) .
- [3] K. Akiyama *et al.* (Event Horizon Telescope), *Astrophys. J. Lett.* **875**, L6 (2019), [arXiv:1906.11243 \[astro-ph.GA\]](#) .
- [4] K. Akiyama *et al.* (Event Horizon Telescope), *Astrophys. J. Lett.* **875**, L5 (2019), [arXiv:1906.11242 \[astro-ph.GA\]](#) .
- [5] S. E. Gralla, D. E. Holz, and R. M. Wald, *Phys. Rev. D* **100**, 024018 (2019), [arXiv:1906.00873 \[astro-ph.HE\]](#) .
- [6] R. Narayan, M. D. Johnson, and C. F. Gammie, *Astrophys. J. Lett.* **885**, L33 (2019), [arXiv:1910.02957 \[astro-ph.HE\]](#) .
- [7] M. D. Johnson *et al.*, *Sci. Adv.* **6**, eaaz1310 (2020), [arXiv:1907.04329 \[astro-ph.IM\]](#) .
- [8] S. E. Gralla, *Phys. Rev. D* **102**, 044017 (2020), [arXiv:2005.03856 \[astro-ph.HE\]](#) .
- [9] S. E. Gralla and A. Lupsasca, *Phys. Rev. D* **102**, 124003 (2020), [arXiv:2007.10336 \[gr-qc\]](#) .
- [10] S. E. Gralla, A. Lupsasca, and D. P. Marrone, *Phys. Rev. D* **102**, 124004 (2020), [arXiv:2008.03879 \[gr-qc\]](#) .
- [11] S. E. Gralla, *Phys. Rev. D* **103**, 024023 (2021), [arXiv:2010.08557 \[astro-ph.HE\]](#) .
- [12] A. Arvanitaki, S. Dimopoulos, S. Dubovsky, N. Kaloper, and J. March-Russell, *Phys. Rev. D* **81**, 123530 (2010), [arXiv:0905.4720 \[hep-th\]](#) .
- [13] J. Preskill, M. B. Wise, and F. Wilczek, *Phys. Lett. B* **120**, 127 (1983).
- [14] L. F. Abbott and P. Sikivie, *Phys. Lett. B* **120**, 133 (1983).
- [15] M. Dine and W. Fischler, *Phys. Lett. B* **120**, 137 (1983).
- [16] R. PENROSE and R. M. FLOYD, *Nature Physical Science* **229**, 177 (1971).
- [17] Y. B. Zel’Dovich, *Soviet Journal of Experimental and Theoretical Physics Letters* **14**, 180 (1971).

- [18] W. H. Press and S. A. Teukolsky, *Nature* **238**, 211 (1972).
- [19] T. Damour, N. Deruelle, and R. Ruffini, *Lett. Nuovo Cim.* **15**, 257 (1976).
- [20] T. J. M. Zouros and D. M. Eardley, *Annals Phys.* **118**, 139 (1979).
- [21] S. L. Detweiler, *Phys. Rev. D* **22**, 2323 (1980).
- [22] M. J. Strafuss and G. Khanna, *Phys. Rev. D* **71**, 024034 (2005), arXiv:gr-qc/0412023 .
- [23] S. R. Dolan, *Phys. Rev. D* **76**, 084001 (2007), arXiv:0705.2880 [gr-qc] .
- [24] R. Brito, V. Cardoso, and P. Pani, *Lect. Notes Phys.* **906**, pp.1 (2015), arXiv:1501.06570 [gr-qc] .
- [25] R. Roy and U. A. Yajnik, *Phys. Lett. B* **803**, 135284 (2020), arXiv:1906.03190 [gr-qc] .
- [26] R. Roy, S. Vagnozzi, and L. Visinelli, *Phys. Rev. D* **105**, 083002 (2022), arXiv:2112.06932 [astro-ph.HE] .
- [27] Y. Chen, R. Roy, S. Vagnozzi, and L. Visinelli, *Phys. Rev. D* **106**, 043021 (2022), arXiv:2205.06238 [astro-ph.HE] .
- [28] A. K. Saha, P. Parashari, T. N. Maity, A. Dubey, S. Bouri, and R. Laha, *Eur. Phys. J. C* **84**, 901 (2024), arXiv:2208.03530 [astro-ph.HE] .
- [29] Y. Chen, J. Shu, X. Xue, Q. Yuan, and Y. Zhao, *Phys. Rev. Lett.* **124**, 061102 (2020), arXiv:1905.02213 [hep-ph] .
- [30] S. M. Carroll, G. B. Field, and R. Jackiw, *Phys. Rev. D* **41**, 1231 (1990).
- [31] D. Harari and P. Sikivie, *Phys. Lett. B* **289**, 67 (1992).
- [32] Y. Chen, Y. Liu, R.-S. Lu, Y. Mizuno, J. Shu, X. Xue, Q. Yuan, and Y. Zhao, *Nature Astron.* **6**, 592 (2022), arXiv:2105.04572 [hep-ph] .
- [33] Y. Chen, C. Li, Y. Mizuno, J. Shu, X. Xue, Q. Yuan, Y. Zhao, and Z. Zhou, *JCAP* **09**, 073 (2022), arXiv:2208.05724 [hep-ph] .
- [34] T. Damour and A. M. Polyakov, *Nucl. Phys. B* **423**, 532 (1994), arXiv:hep-th/9401069 .
- [35] M. B. Green, J. H. Schwarz, and E. Witten, *SUPERSTRING THEORY. VOL. 1: INTRODUCTION*, Cambridge Monographs on Mathematical Physics (1988).
- [36] C. Wetterich, *Nucl. Phys. B* **302**, 668 (1988), arXiv:1711.03844 [hep-th] .
- [37] M. Gasperini, F. Piazza, and G. Veneziano, *Phys. Rev. D* **65**, 023508 (2002), arXiv:gr-qc/0108016 .
- [38] D. Tocchini-Valentini and L. Amendola, *Phys. Rev. D* **65**, 063508 (2002), arXiv:astro-ph/0108143 .
- [39] A. C. Davis, P. Brax, and C. van de Bruck, *Nucl. Phys. B Proc. Suppl.* **148**, 64 (2005), arXiv:astro-ph/0503467 .
- [40] J. D. Bekenstein, “Fine-structure constant: Is it really a constant?” in *Jacob Bekenstein: The Conservative Revolutionary*, edited by L. Brink, V. Mukhanov, E. Rabinovici, and K. K. Phua (World Scientific, Singapur, 2020) pp. 347–359.
- [41] H. B. Sandvik, J. D. Barrow, and J. Magueijo, *Phys. Rev. Lett.* **88**, 031302 (2002), arXiv:astro-ph/0107512 .
- [42] Y. V. Stadnik and V. V. Flambaum, *Phys. Rev. Lett.* **115**, 201301 (2015), arXiv:1503.08540 [astro-ph.CO] .
- [43] D. R. Brill, P. L. Chrzanowski, C. Martin Pereira, E. D. Fackerell, and J. R. Ipser, *Phys. Rev. D* **5**, 1913 (1972).
- [44] B. Carter, *Commun. Math. Phys.* **10**, 280 (1968).

- [45] I. M. Ternov, V. R. Khalilov, G. A. Chizhov, and A. B. Gaina, *Sov. Phys. J.* **21**, 1200 (1978).
- [46] D. Baumann, H. S. Chia, J. Stout, and L. ter Haar, *JCAP* **12**, 006 (2019), [arXiv:1908.10370 \[gr-qc\]](#) .
- [47] L. D. Landau and E. M. Lifshitz, *Fluid Mechanics: Volume 6*, Vol. 6 (Elsevier, 1987).
- [48] K. S. Thorne, C. W. Misner, and J. A. Wheeler, *Gravitation* (Freeman San Francisco, 2000).
- [49] J. D. Jackson, *Classical electrodynamics* (John Wiley & Sons, 1998).
- [50] J. Frank, A. R. King, and D. Raine, *Accretion power in astrophysics* (Cambridge university press, 2002).
- [51] R. A. Breuer and J. Ehlers, Proceedings of the Royal Society of London. A. Mathematical and Physical Sciences **370**, 389 (1980).
- [52] R. Narayan and I. Yi, *apjl* **428**, L13 (1994), [arXiv:astro-ph/9403052 \[astro-ph\]](#) .
- [53] Y. Huang, Y.-P. Dong, and D.-J. Liu, *Int. J. Mod. Phys. D* **27**, 1850114 (2018), [arXiv:1807.06268 \[gr-qc\]](#) .
- [54] V. Perlick, O. Y. Tsupko, and G. S. Bisnovaty-Kogan, *Phys. Rev. D* **92**, 104031 (2015), [arXiv:1507.04217 \[gr-qc\]](#) .
- [55] J. Synge, *Relativity: The General Theory*, North-Holland series in physics No. 1 (North-Holland Publishing Company, 1960).
- [56] F. C. Michel, *apss* **15**, 153 (1972).
- [57] K. Akiyama *et al.* (Event Horizon Telescope), *Astrophys. J. Lett.* **930**, L12 (2022), [arXiv:2311.08680 \[astro-ph.HE\]](#) .
- [58] A. M. Ghez, S. Salim, N. N. Weinberg, J. R. Lu, T. Do, J. K. Dunn, K. Matthews, M. R. Morris, S. Yelda, E. E. Becklin, T. Kremenek, M. Milosavljevic, and J. Naiman, *apj* **689**, 1044 (2008), [arXiv:0808.2870 \[astro-ph\]](#) .
- [59] J. A. Davidson, M. W. Werner, X. Wu, D. F. Lester, P. M. Harvey, M. Joy, and M. Morris, *apj* **387**, 189 (1992).
- [60] K. Akiyama *et al.* (Event Horizon Telescope), *Astrophys. J. Lett.* **875**, L6 (2019), [arXiv:1906.11243 \[astro-ph.GA\]](#) .
- [61] K. Gebhardt and J. Thomas, *The Astrophysical Journal* **700**, 1690 (2009).
- [62] L. C. Ho, *The Astrophysical Journal* **699**, 626 (2009).
- [63] R. Narayan and I. Yi, *apj* **452**, 710 (1995), [arXiv:astro-ph/9411059 \[astro-ph\]](#) .
- [64] G. S. Bisnovaty-Kogan and R. V. E. Lovelace, *Astrophys. J.* **529**, 978 (2000), [arXiv:astro-ph/9902344](#) .
- [65] H. Falcke, F. Melia, and E. Agol, *apjl* **528**, L13 (2000), [arXiv:astro-ph/9912263 \[astro-ph\]](#) .